J Solid State Electrochem (2007) 11:1375–1384
DOI 10.1007/s10008-007-0316-2

ORIGINAL PAPER

Dielectric properties of Al–Si composite oxide films formed on electropolished and DC-etched aluminum by electrophoretic sol-gel coating and anodizing

M. Sunada · H. Takahashi · T. Kikuchi · M. Sakairi · S. Hirai

Received: 27 December 2006 / Revised: 6 February 2007 / Accepted: 22 March 2007 / Published online: 26 April 2007

Abstract Highly pure aluminum specimens (99.99%) after electropolishing and DC-etching were covered with SiO_2 films by electrophoretic sol-gel coating and were anodized in neutral boric acid/borate solutions. Time-variations in cell voltage during electrophoretic sol-gel coating and in anode potential during anodizing were monitored. Structure and dielectric properties of the anodic oxide films were examined by scanning electron microscopy (SEM), transmission electron microscopy (TEM), energy-dispersive X-ray (EDX), and electrochemical impedance spectroscopy (EIS). It was found that electrophoretic sol-gel coating forms uniform SiO_2 films on the surface of both electropolished and DC-etched specimens. Anodizing of specimens after electrophoretic coating lead to the formation of anodic oxide films consisting of two layers: an inner alumina layer and an outer Al–Si composite oxide layer. The anodic oxide films formed, thus, had slightly higher capacitances than those formed on aluminum without any coating. Higher heating temperatures after electrophoretic deposition caused the increase in capacitance of anodic oxide films more effectively. Anodizing in a boric acid solution after SiO_2 coating on DC-etched foil allowed the anode potential to reach a value higher than 1,000 V, resulting in 39% higher capacitances than those on specimens without SiO_2 film.

Keywords Aluminum · Electrolytic capacitor · Electrophoretic deposition · Sol-gel coating · Composite oxide film

Dedicated to Professor Su-Il Pyun on the occasion of his 65th birthday.

M. Sunada · H. Takahashi (✉) · T. Kikuchi · M. Sakairi
Graduate School of Engineering, Hokkaido University, Sapporo, Japan
e-mail: takahasi@elechem1-mc.eng.hokudai.ac.jp

S. Hirai
Facaulty of Engineering, Muroran Institute of Technology, Muroran, Japan

Introduction

Aluminum electrolytic capacitors, which use aluminum anodic oxide films as a dielectric layer, have high electric capacitance, self-repairing ability, and high voltage sustainability, and are used in many electric circuits with switching regulator, AC–DC inverter, and others. Recent development in hybrid and electric vehicle strongly requires small electrolytic capacitors with high electric capacitance and high voltage sustainability. The capacitance, C, of the electrolytic capacitor can be expressed by the following equation:

$$C = \varepsilon_0 \varepsilon S/\delta \quad (1)$$

where ε_0 is the vacuum permittivity, ε the relative dielectric constant of anodic oxide films, S the surface area, and δ the film thickness. This equation indicates that C value is directly proportional to the dielectric constant of oxide films and surface area and inversely proportional to the film thickness.

Increase in S is attained by electrochemical etching of the aluminum substrate before anodizing in electrolytic capacitor manufacturing industry. Etching with direct current (DC-etching) is used for high voltage sustainable capacitors while alternative current etching (AC-etching) for low voltage sustainable capacitors. Decrease in δ can be achieved by forming anodic oxide films with low K values [1–6]. The K value is defined as the ratio of film thickness against film formation potential (δ/E_a). Anodic oxide films containing crystalline oxides have low K values, as strong

chemical bonds in crystalline oxides may enable higher electric fields across the oxide. Increase in ε values of anodic oxide films can be only slightly achieved by the formation of crystalline oxides but may be achieved vigorously by incorporating metal oxides, which have high ε *values* [7–13].

In previous studies, the authors developed a new process, which was anodizing after sol-gel dip coating of valve metal oxides [14–22]. It was found in the study that anodizing of Al specimens after SiO_2-coating by sol-gel dip coating causes the formation of anodic oxide films including an Al–Si composite oxide layer. This film had high voltage sustainability and at most about 20% higher parallel capacitance than anodic oxide films on electropolished aluminum without any coating. However, the sol-gel dip coating was insufficient for uniform coating of SiO_2 films on DC-etched aluminum with micro-tunnel pits.

In the present investigation, the authors attempt to form Al–Si composite oxide films by electrophoretic sol-gel coating [23–25] and anodizing on both electropolished and DC-etched aluminum foil to examine dielectric properties of the composite oxide film.

Experimental

Specimens

Highly pure aluminum foil (99.99%) was used as specimens after electropolishing (specimen-I) or DC-etching (specimen-II, supplied by Nippon Chemi-Con). In a preliminary experiment, both types of specimens were anodized at 5 V in 0.5 kmol m^{-3}–H_3BO_3/0.05 kmol m^{-3}–$Na_2B_4O_7$ solution to compare the parallel capacitance of anodic oxide films on specimen-I with that on specimen-II. It was assumed from the preliminary experiment that the surface area of specimen-II is 20 times as large as that of specimen-I. In the present study, currents in electrophoretic sol-gel deposition and anodizing were determined so that the current density is the same on both types of specimens. The size of specimens exposed to the solutions during electrophoretic deposition and anodizing was 4×10^{-4} m^2 on specimen-I and 0.4×10^{-4} m^2 on specimen-II.

Specimen-I, which had been electropolished in a $HClO_4$/CH_3COOH solution, was dipped in ethanol and kept in a silica gel desiccator before sol-gel coating, while specimen-II, which had been DC-etched, was dipped in ethanol and kept in a vacuum desiccator.

SiO_2-film coating by electrophoretic sol-gel method

A sol composed of tetra-ethoxysilane [$Si(OC_2H_5)_4$], NH_3, distilled water and dehydrated ethanol (1:0.07:5.75:17.6 in molar ratio) was prepared in a glove box at room temperature under N_2 atmosphere. Relative humidity in the grove box was kept below 2.0% [17]. Specimen-I or specimen-II as an anode and a platinized Pt electrode as a cathode were dipped into the sol, and constant currents of $i_c=0.05-0.2$ A m^{-2} were applied until cell voltage, V_c, reaches a preset value. After the electrophoretic deposition, the specimens were withdrawn from the sol at 0.3 mm s^{-1}, dried at 298 K for 300 s, and heated at $T_h=573$, 673, and 773 K for $t_h=1.8$ ks in O_2 atmosphere [17]. After coatings, mass gains of the specimens were measured by a microbalance. In a part of experiments, the process of electrophoretic deposition, drying, and heating were repeated at most $n=2$ times.

Sol-gel dip coating was also carried out to compare the uniformity of SiO_2 film coated by electrophoretic coating with that by dip coating. In the dip coating, specimen-I and specimen-II were immersed into the sol for 300 s on open circuit, and then dried/heated under the same conditions as the electrophoretic coating.

Anodizing

The specimens coated with SiO_2 film were anodized with a constant current of $i_a=10$ A m^{-2} at $T_a=293$ K in 0.5 kmol m^{-3}–H_3BO_3/0.05 kmol m^{-2}–$Na_2B_4O_7$ solution (solution-I) and 0.5 kmol m^{-3}–H_3BO_3 solution (solution-II). Specimens without SiO_2-films were also anodized under the same conditions. The change in anode potential, E_a (vs Ag/AgCl), with time, t_a, during anodizing was monitored by a digital multi-meter connected to a PC system. The measurement of E_a was carried out with a three electrode system consisting of Pt counter electrode and Ag/AgCl reference electrode, as well as Al working electrode during anodizing in solution-I, while during anodizing in solution-II, a two electrode system consisting of Al working electrode and Pt counter electrode was used to estimate E_a by subtracting the solution potential drop from cell voltage. The application of the two-electrode system is because of avoidance of the current flow through reference electrode due to the increase in anode potentials up to as high as 1,000 V during anodizing in solution-II.

Characterization

Sections of anodic oxide films formed after SiO_2-coating were examined by transmission electron microscopy (TEM, Hitachi H-700H) using an ultra thin sectioning technique and analyzed with energy dispersed X-ray analyzer (EDX, JEOL JEM-2000ES). The surface of specimens after SiO_2-coating and anodizing was observed by scanning electron microscopy (FE-SEM, JEOL JSM-6300 F). A thin layer of platinum was coated on the specimens before SEM.

Electrochemical impedance spectroscopy (EIS, NF-S5720B) was performed in 0.5 kmol m^{-3}–H_3BO_3/0.05 kmol m^{-2}–$Na_2B_4O_7$ solution using sinusoidal wave of 10 mV amplitude.

Frequency range of the signal was 0.1 Hz~50 kHz. Parallel capacitances of anodic oxide films, C_p, were estimated by analyzing Bode diagrams of EIS.

Results and discussion

SiO_2 films coated by electrophoretic deposition

Figure 1 shows the time-variations in cell voltage, V_c, during electrophoretic deposition of SiO_2 with different current densities of i_c=0.01–0.2 A m^{-2} on (a) specimen-I and (b) specimen-II. On specimen-I and specimen-II, V_c shows a jump at the initial stage of deposition, and then increases linearly with coating time, t_c. With increasing i_c, the V_c jump becomes more remarkable, and the slope of V_c vs t_c curves becomes steeper. The voltage jump at the initial stage on specimen-II is higher than that on specimen-I and that the slope of V_c vs t_c curve on specimen-II is as high as that of specimen-I at each i_c. This suggests that the V_c jump is due to IR-drop of sol, and the increase in V_c with t_a is due to the deposition of SiO_2 sol and the formation of anodic oxide films. The larger IR-drop of sol on specimen-II is considered to be due to its micro-pit structure.

Figure 2 shows the effect of heating temperature, T_h, on the V_c vs t_c curve during the second step (n=2) on specimen-I with i_c=0.2 A m^{-2}. In the first step, SiO_2 gel was deposited with i_c=0.2 A m^{-2} up to E_c=5 V, and then, heat treatment was carried out at T_h=573, 673, and 773 K for t_h=1.8 ks. Each curve shows a jump of V_c at the initial stage of the deposition, and then a rapid decrease in V_c before reaching a steady value. After the steady V_c between 10 and 150 s, V_c increases linearly with coating time, t_c. It can be seen from Fig. 3 that higher T_hs lead to higher steady values of V_c, shorter steady V_c periods, and flatter slopes of V_c vs t_c curves after the steady period. Higher heating temperatures is considered to cause more evaporation of organic compounds and dehydration of SiO_2 gel, resulting in the formation of more anhydrous SiO_2 with more micro-cracks, although the effect of heating temperature, T_c, in the first coating process on the second coating process has not been examined further.

Figure 3 shows the TEM images of the cross-section of specimen-I after electrophoretic deposition up to V_c=10 V by (a) one step (n=1, see Fig. 1a) and (b) two steps (n=2, see Figs. 1a and 2). Both specimens were heated at T_h=573 K for t_h=1.8 ks after each deposition step. There are two layers on the specimen surface in both photos: an inner dark layer with 15-nm thickness and an outer gray layer

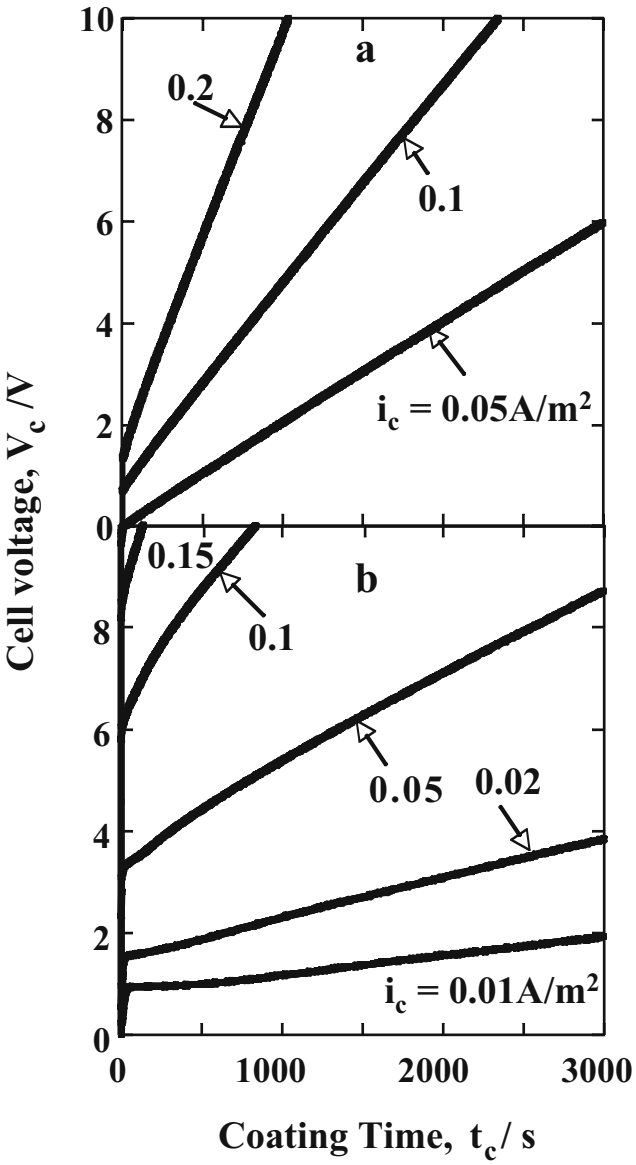

Fig. 1 Time-variations in cell voltage, V_c, during electrophoretic deposition of SiO_2 with different current densities of i_c=0.01–0.2 A m^{-2} on **a** specimen-I and **b** specimen-II

with 50–80 nm thickness. The outer layer is SiO_2 layer deposited from sol, and the inner layer is the oxide layer formed by anodic oxidation, which may consist of Al–Si composite oxide. The SiO_2 layer is thinner on the specimen coated by one step than by two steps, while the thickness of the Al–Si composite oxide layer does not depend on the repetition number, n. Judging from the inner layer thickness, one can assume that the anodic oxide layer sustains the most of cell voltage during electrophoretic deposition.

Figure 4 shows the TEM images of the cross-sections of specimen-II after (a) dip coating (low magnification), (b) dip coating (high magnification), (c) electrophoretic coating (low magnification), and (d) electrophoretic coating (high magnification). In both processes, heating was carried out

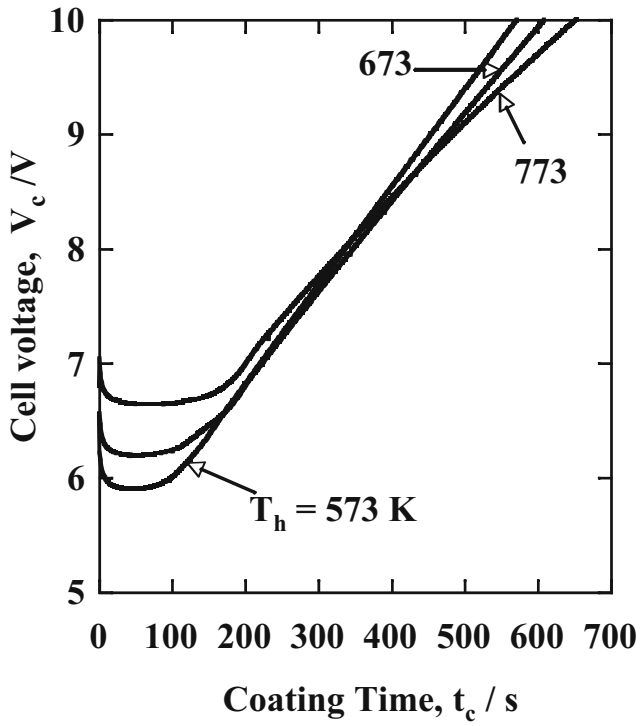

Fig. 2 Change in cell voltage, V_c, with time, t_c, during the second electrophotretic sol-gel coating obtained for specimen-I. In the first step, SiO_2 gel was deposited with i_c=0.2 A m^{-2} up to E_c=5 V, and then heat treatment was carried out at T_h=573, 673, and 773 K for t_h=1.8 ks

at T_h=573 K for t_h=1.8 ks, and in the electrophoretic deposition, the coating was carried out up to V_c=10 V. Fig. 4a and b shows that many tunnel-pits of etched specimens are filled with an epoxy resin used for specimen embedding instead of SiO_2. It can be seen from Fig. 4c and d that the electrophoretic deposition enables the relatively uniform coating of SiO_2 on the inner wall of tunnel-pits.

Figure 5 shows SEM images of the surface of specimen-II (a) before SiO_2 coating, (b) after SiO_2 coating by dipping, (c) after coating by electrophoretic deposition up to V_c=10 V with n=1, and (d) after coating by electrophoretic deposition up to V_c=10 V with n=2. Specimens were heated at T_h=573 K for t_h=1.8 ks after electrophoretic and dip coating. The surface of the specimen-II before SiO_2 coating (Fig. 5a) appears very smooth, while the surface after SiO_2 coating (Fig. 5b, c, and d) appears rough due to the deposition of SiO_2. Comparing Fig. 5b with c and d strongly suggest that electrophoretic deposition results in much more uniform coating than dip process.

Table 1 shows the mass gain of specimen-I and specimen-II by dip coating and electrophoretic coating with i_c=0.05, 0.1 and 0.2 A m^{-2}. After dip and electrophoretic deposition, the specimens were heated at T_h=573 K for t_h= 1.8 ks in O_2 atmosphere. The mass gain of each specimen by electrophoretic deposition is much larger than that by dip coating, suggesting that the effect of electric field is significant for uniform coating of SiO_2. Mass gain by electrophoretic process does not depend on current density on specimen-I, while it slightly decreases with increasing c. d. on specimen-II.

The amount of O^{2-} ions in anodic oxide films formed by electrophoretic coating can be estimated from Fig. 3a to be ca. 0.014 g m^{-2}, assuming that the inner layer is composed of Al_2O_3 with a density of 3,000 kg m^{-3}. This amount corresponds to only 10% of mass gain on specimen-I and 4% on specimen-II. The mass gain by electrophoretic coating on specimen-II is much larger than that on specimen-I, suggesting that excess sol in micro-pits of specimen-II leads to the larger mass gain.

Anodic oxide film formation on SiO_2-coated specimen in solution-1

Figure 6 shows the E_a vs t_a curves obtained in solution-1 on (a) specimen-I and (b) specimen-II, which were coated with SiO_2 layers at i_c=0.05–0.2 A m^{-2} before heat treatment at T_h=573 K for t_h=1.8 ks. The E_a vs t_a curve for specimen-I and specimen-II without any coating is also indicated as broken lines. Specimen-I coated with SiO_2 shows a 10 V jump in E_a at the initial stage and then linear increase in E_a with t_a. The slope of E_a vs t_a curves for specimen-I with SiO_2-coating is slightly steeper than that without SiO_2-coating and does not depend on i_c. The steeper slopes of the

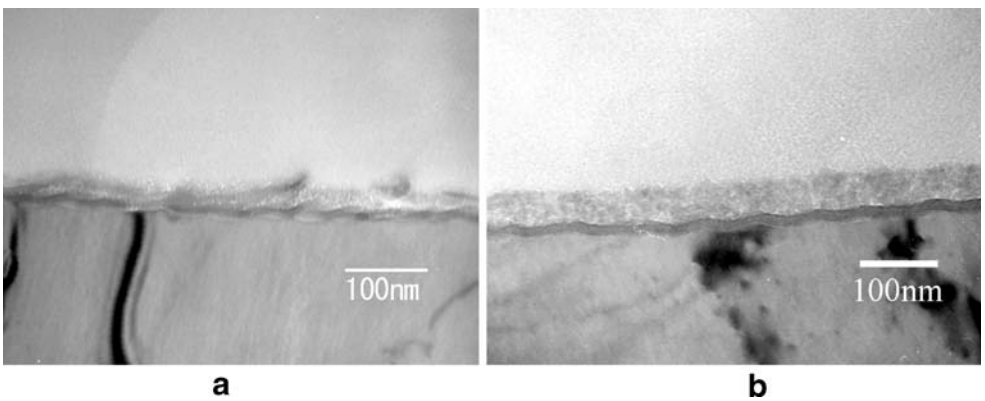

Fig. 3 TEM images of the cross-section of specimen-I after electrophoretic deposition up to V_c=10 V by **a** one step and **b** two steps. Both specimens were heated at T_h=573 K for t_h=1.8 ks after each deposition step

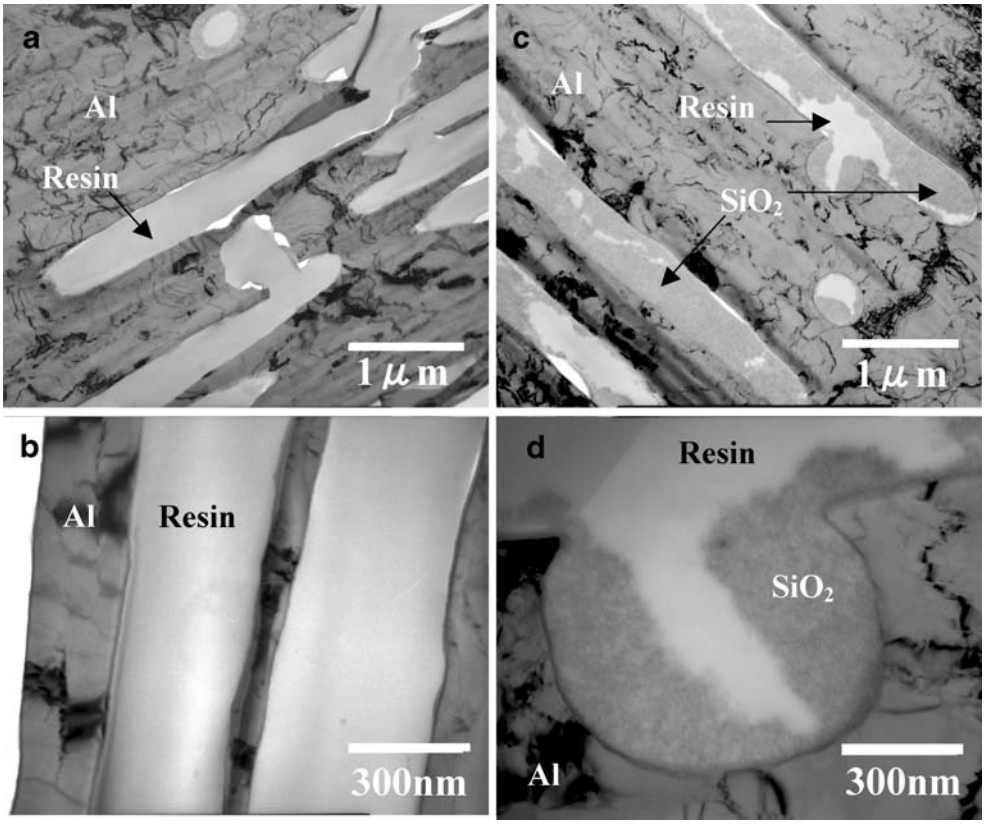

Fig. 4 TEM images of the cross-sections of specimen-II after **a** dip coating (low magnification), **b** dip coating (high magnification), **c** electrophoretic coating (low magnification), and **d** electrophoretic deposition (high magnification). In both processes, heating was carried out at T_h=573 K for t_h=1.8 ks, and in the electrophoretic deposition, the coating was carried out up to V_c=10 V

E_a vs t_a curves on SiO_2-coated specimen-I suggest the formation of Al–Si composite oxide films. All the E_a vs t_a curves in specimen-II (Fig. 6b) show a slightly upwards curved line unlike in specimen-I, and this is because the surface area of specimens decreases gradually with increasing E_a on specimen-II, due to the filling of micro-tunnel pits

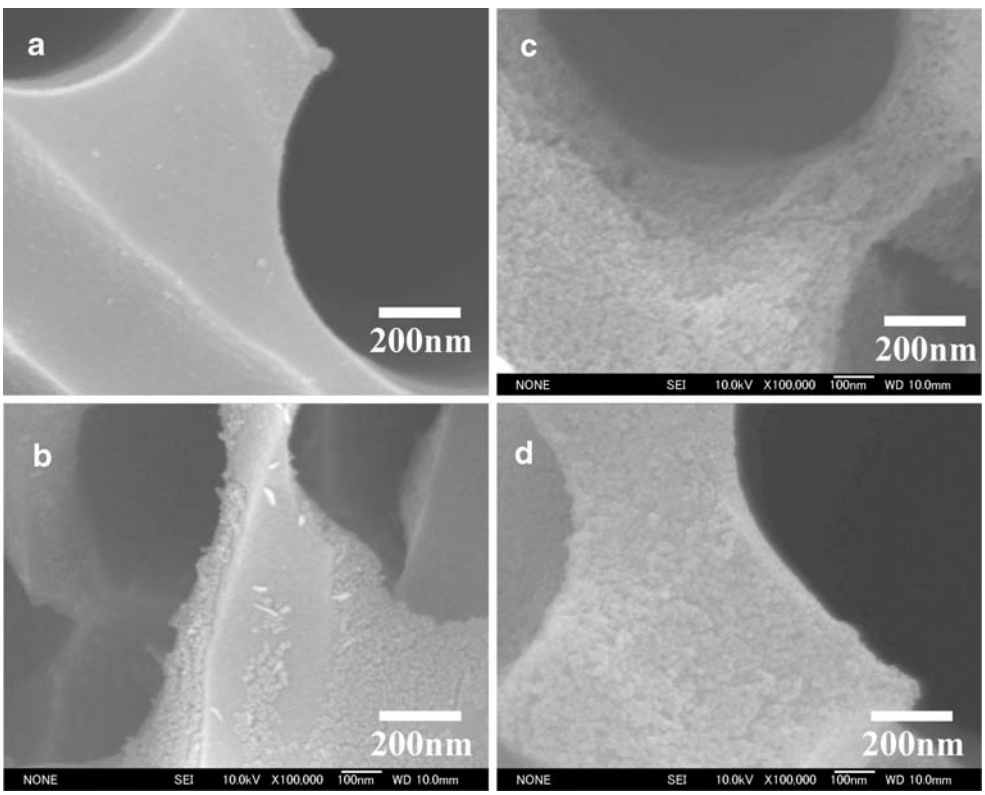

Fig. 5 SEM images of the surface of specimen-II **a** before SiO_2 coating, **b** after SiO_2 coating by dipping process, **c** after coating by electrophoretic deposition up to V_c=10 V with n=1, and **d** after coating by electrophoretic deposition up to V_c= 10 V with n=2. Specimens were heated at T_h=573 K for t_h= 1.8 ks after electrophoretic and dip coating

Table 1 Mass gain of specimen-I and specimen-II during dip-coating and electrophoretic coating up to 10 V

Specimen	Mass gain (g m^{-2})			
	Dipping (t=1.8 ks)	Electrophoretic		
		i_c=0.05 A m^{-2}	i_c=0.1 A m^{-2}	i_c=0.2 A m^{-2}
I	0.03	0.15	0.13	0.15
II	0.05	0.36	0.35	0.31

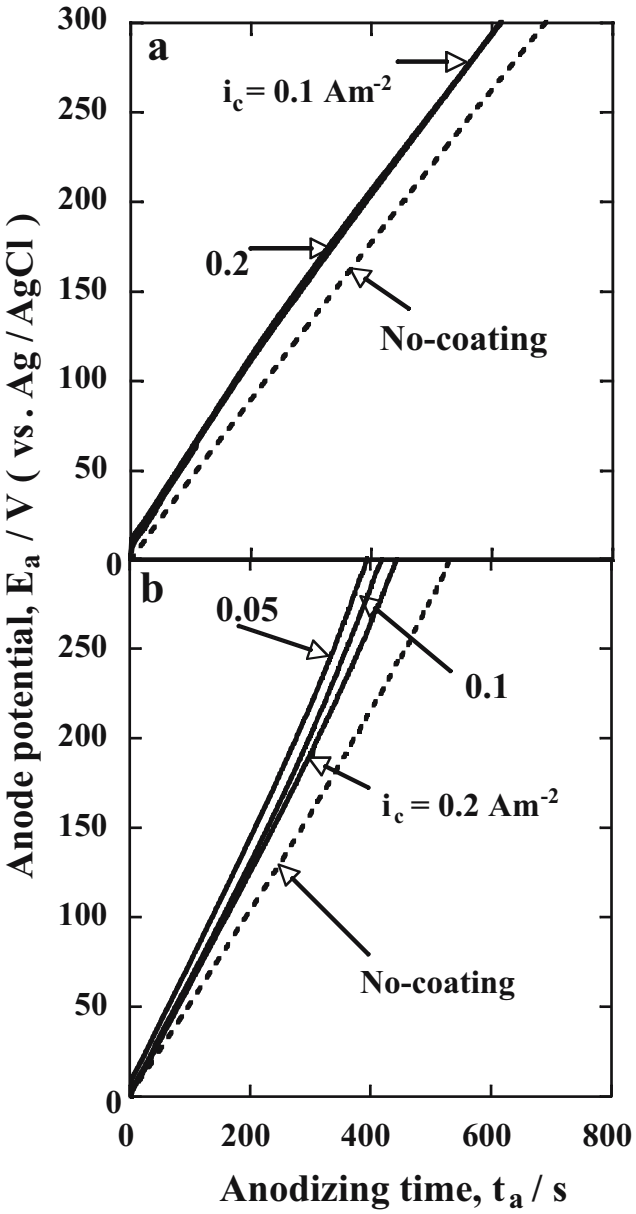

Fig. 6 Time-variations in anode potential, E_a, during anodizing in solution-I before/after SiO_2 coating obtained for **a** specimen-I and **b** specimen-II. The SiO_2 coating was carried out at i_c=0.05, 0.1 and 0.2. A m^{-2} before heat treatment at T_h=573 K for t_h=1.8 ks

with anodic oxide films. The slope of the curves on SiO_2-coated specimen-II is steeper than that on SiO_2-coated specimen-I and becomes steeper at lower i_c. Smaller i_c seems to allow the formation of Al–Si composite oxide films more uniformly on the inner wall of tunnel pits of specimen-II. This can be expected from larger mass gains in electrophoretic coating at smaller i_c (see Table 1).

Figure 7 shows the effect of heating temperature, T_h, and repetition number of coating, n, on E_a vs t_a curve on specimen-II. Current density during electrophoretic deposition, i_c, was 0.05 A m^{-2} on all the specimens examined in this study, and in the case of n=2, the procedure of SiO_2 coating is the same as that shown in Fig. 6. It can be seen from Fig. 7 that T_h=773 K gives the steepest slope of E_a vs t_a curves and that the effect of T_h and n on the anodizing behavior is not significant at temperatures below T_h<673 K. The steepest slope with T_h=773 K is difficult to explain, but it can be expected that higher heating temperature causes the formation of more anhydrous SiO_2, leading to the enhancement of Al–Si composite oxide layer formation during anodizing.

Figure 8 shows TEM images of the vertical cross-sections of specimen-I with SiO_2-coating and anodizing up to (a) 100, (b) 200, and (c) 300 V. The SiO_2-coating were carried out with i_c=0.2 A m^{-2} up to V_c=10 V before heating at T_h=573 K for t_h=1.8 ks. All the films show two layers underneath SiO_2 layer: an outer layer and an inner layer. EDX analysis showed that the inner layer is composed of alumina, and the outer layer is composed of Al–Si composite oxide. Both layers become thicker with E_a, while SiO_2 layer becomes thinner. This can be explained in terms of the conversion of SiO_2 to Si–Al composite oxide and the formation of Al_2O_3 [17]. The sum of the thickness of the outer and inner layers at E_a=300 V is ca. 330 nm, indicating 1.1 nm/V of K value, which is much smaller than 1.5 nm/V for anodic oxide films formed on electropolished aluminum. This is due to the high electric field sustainability of Al–Si composite oxide layer.

Figure 9 shows the TEM image of the cross-section of specimen-II after electrophoretic coating and anodizing. Electrophoretic coating was carried out under the conditions of i_c=0.05 A m^{-2}, V_c=10 V, T_h=573 K, and t_h=1.8 ks, and anodizing was carried out up to E_a=100 V in solution-I.

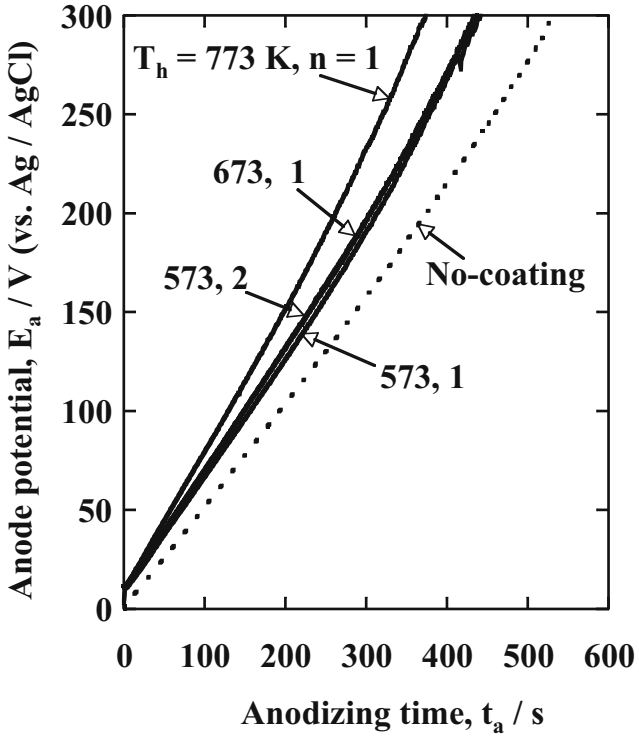

Fig. 7 Effect of heating temperature, T_h, and repetition number of coating, n, on E_a vs t_a curve on specimen-II. Electrophoretic deposition was carried out with i_c=0.05 A m^{-2} up to 10 V

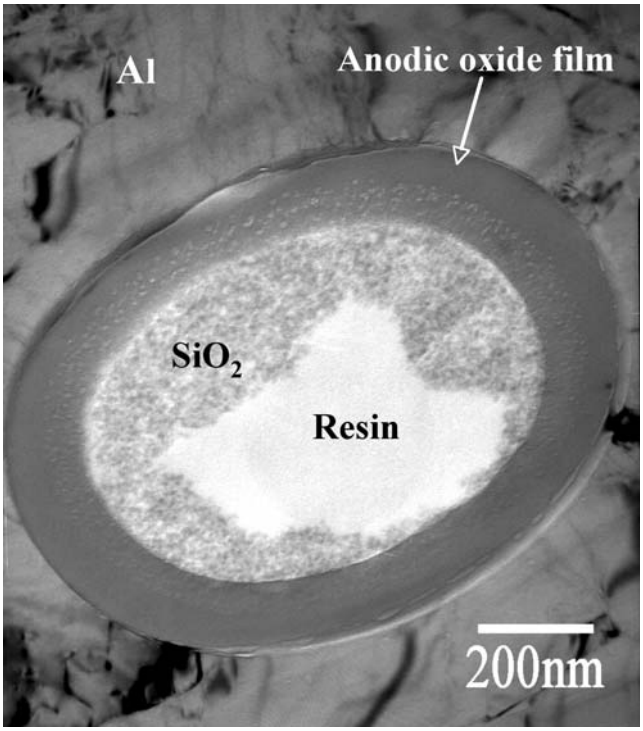

Fig. 9 TEM image of the cross-section of specimen-II after electrophoretic coating and anodizing. Electrophoretic coating was carried out under the conditions of i_c=0.05 A m^{-2}, V_c=10 V, T_h= 573 K, and t_h=1.8 ks, and anodizing was carried out up to E_a=100 V in solution-I

There appears an anodic oxide film on the inner wall of a tunnel pit, which was cut into round slices. Agglomerated SiO_2 is observed on the anodic oxide film at the inside of the tunnel pit, and its thickness is not uniform. The anodic oxide film is composed of two layers: an inner structure-less layer and an outer small particle-dispersed layer. The inner layer may be composed of Al_2O_3 and the outer layer of Al–Si composite oxide.

Dielectric properties of anodic oxide films formed on SiO_2 coated specimen

Figure 10 shows the relationship between the reciprocal of parallel capacitance, $1/C_p$, of anodic oxide films and anode potential, E_a, obtained for specimen-I coated with SiO_2 at i_c=0.2 A m^{-2} up to V_c=10 V and T_h=573, 673, and 773 K. Anodizing condition is as described in the experimental section [i_a=10 A m^{-2}, T_a=293 K, 0.5 kmol m^{-3}–H_3BO_3/0.05 kmol m^{-3}–$Na_2B_4O_7$ (solution-I)]. The $1/C_p$ values of all the specimens are proportional to E_a. The T_c=573 K specimen has the same slope as the

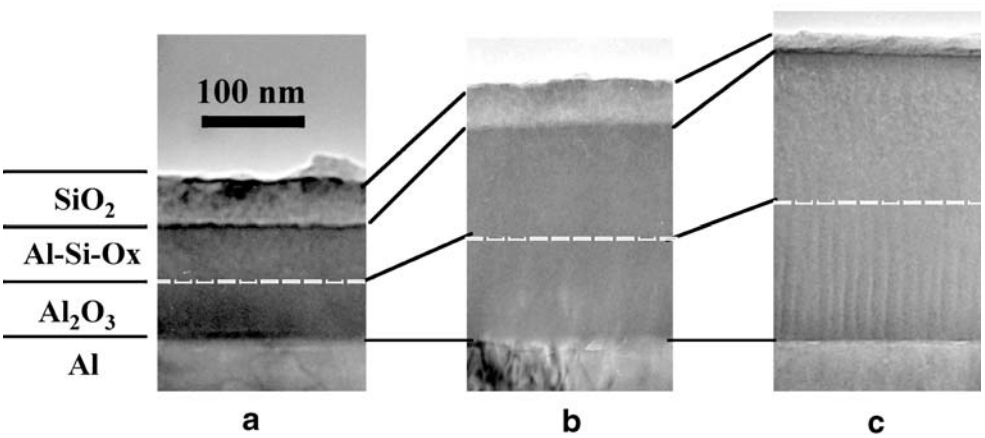

Fig. 8 TEM images of the vertical cross-sections of specimen-I after SiO_2-coating and anodizing up to **a** 100 V, **b** 200 V, and **c** 300 V. The SiO_2-coating were carried out with i_c=0.2 A m^{-2} up to V_c=10 V before heating at T_h=573 K for t_h=1.8 ks

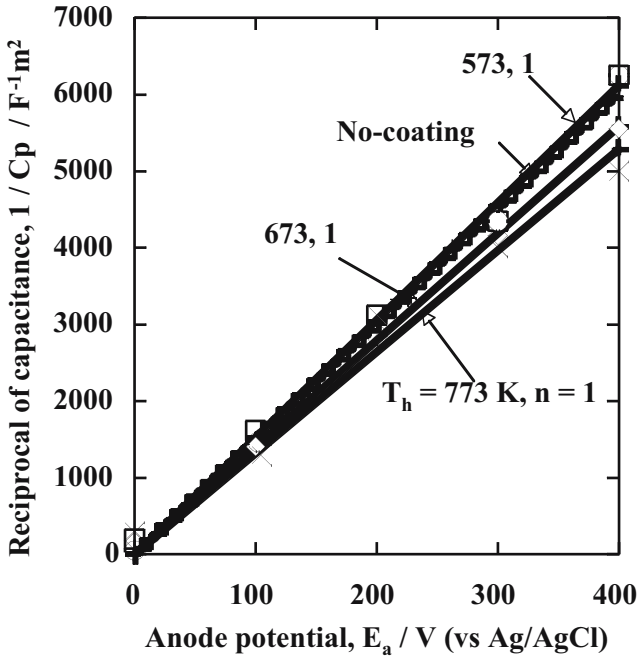

Fig. 10 Relationship between the reciprocal of parallel capacitance, $1/C_p$, of anodic oxide films and anode potential, E_a, obtained for specimen-I coated with SiO_2 at i_c=0.2 A m^{-2} up to V_c=10 V and T_h= 573, 673, and 773 K

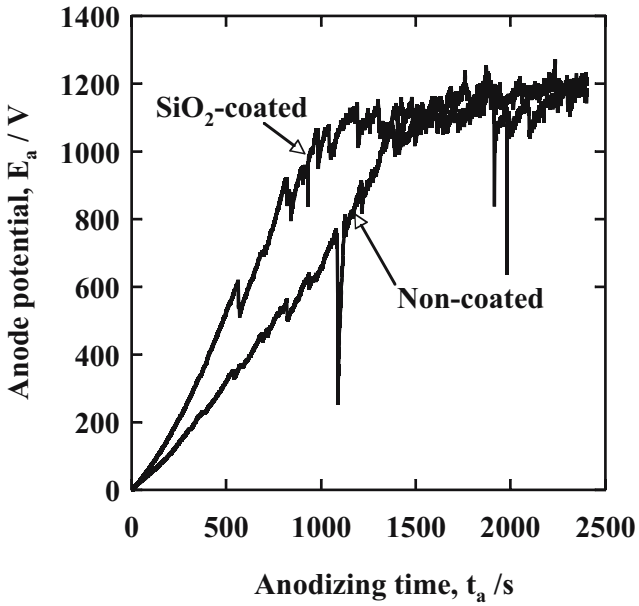

Fig. 11 Changes in anode potential, E_a, with time, t_a, during anodizing of specimen-II in solution-II before/after SiO_2 coating. The SiO_2 coating was carried out by two-step process: the first electrophoretic deposition with 0.2 A m^{-2} up to 20.5 V before heating at T_h=573 K for t_h=1.8 ks and the second electrophoretic deposition with 0.2 A m^{-2} up to 24.5 V before heating under the same conditions

specimen without coating, while specimens with higher T_hs have flatter slopes. This indicates that anodic oxide films formed on specimen-I with SiO_2 films have higher parallel capacitances and that the tendency is pronounced at higher heating temperatures, showing 20% at T_h= 773 K.

The $1/C_p$ vs E_a curves obtained for specimen-II coated with SiO_2 at i_c=0.05 A m^{-2} and T_h=573, 673, and 773 K showed straight lines passing the origin, and the slope of the curves was flatter at higher T_hs. The C_p of anodic oxide films formed on specimen-II after SiO_2 coating at T=773 K was 7% larger than that on specimen-II without coating.

Anodic oxide films formed in solution-II after SiO_2 coating on specimen-II

Anodizing of aluminum in solution-II enables the formation of anodic oxide films with a film breakdown potential as high as 1,000 V [26–28]. The authors, in this study, show the effect of SiO_2 coating on the formation and dielectric properties of such anodic oxide films on specimen-II. Figure 11 shows the changes in anode potential, E_a, with time, t_a, during anodizing of specimen-II in solution-II before/after SiO_2 coating. The SiO_2 coating was carried out by two-step process: the first electrophoretic deposition with 0.2 A m^{-2} up to 20.5 V before heating at T_h=573 K for t_h=1.8 ks and the second electrophoretic deposition with 0.2 A m^{-2} up to 24.5 V before heating under the same conditions. It can be seen from Fig. 11 that E_a increases with t_a on both non-coated and SiO_2-coated specimens, and that the slope of E_a vs t_a curves becomes flatter at E_a= 1,050 V, due to the start of film breakdown. Both curves show oscillation in potential, and the oscillation becomes more remarkable with increasing E_a, especially after film breakdown starts. Before film breakdown, the SiO_2-coated specimen shows steeper slope of the E_a vs t_a curve than noncoated one and smaller potential oscillation.

Figure 12 shows SEM images of the surface of specimen-II (a) before anodizing (no coating), (b) before anodizing (SiO_2 coating), (c) after anodizing up to 1,000 V (no coating), and (d) after anodizing up to 1,000 V (SiO_2 coating). Specimen-II as received (Fig. 12a) shows many pits with sharp edges, while on the specimen after SiO_2 coating (Fig. 12b), there are pits filled with SiO_2 and pit edges are slightly milder than those on the specimen as received. After anodizing up to 1,000 V of specimen-II with/without SiO_2 coating (Fig. 12c and d), most of the pits are filled with anodic oxide films, and edge pits is much milder than those on the specimen before anodizing (Fig. 12a and b). Comparison of Fig. 12c with d shows that the tendency of pit filling and pit-edge mildening is more obvious on noncoated specimen than SiO_2-coated one. This may be due to the formation of thinner anodic oxide films on SiO_2-coated specimen than on non-coated specimen.

Figure 13 shows the relationship between the reciprocal of parallel capacitance, $1/C_p$, with film formation potential,

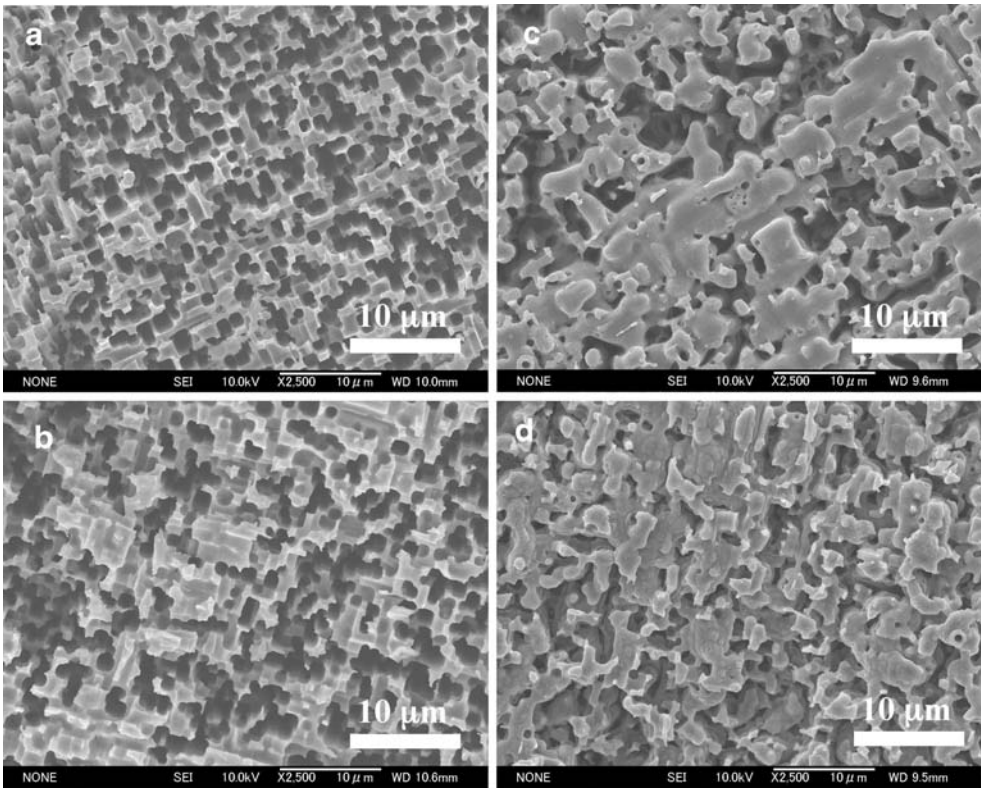

Fig. 12 SEM images of the surface of specimen-II **a** as received **b** after SiO_2 coating, **c** after anodizing up to 1,000 V without any coating, and **d** after SiO_2 coating and anodizing up to 1,000 V

E_a, obtained for specimen-II with/without SiO_2 coating. The $1/C_p$ vs E_a curves of both specimens show the upwards curved shape with increasing E_a, unlike the straight lines in Fig. 10, where $1/C_p$ is proportional to E_a. This is due to the decrease in surface area by filling of tunnel pits with anodic oxide films on specimen-II, and the tendency becomes much more remarkable as E_a rises above 500 V.

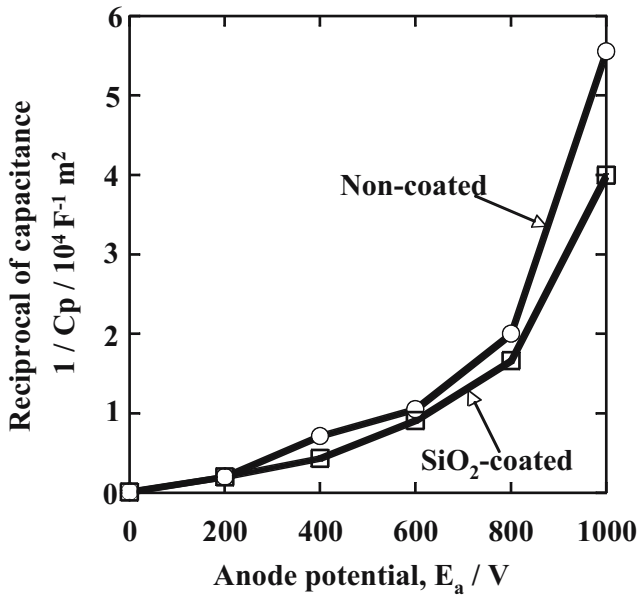

Fig. 13 Relationship between the reciprocal of parallel capacitance, $1/C_p$, with film formation potential, E_a, obtained for specimen-II with/without SiO_2 coating

It should be emphasized here that the value of $1/C_p$ for SiO_2-coated specimen at each E_a is smaller than that for non-coated specimen. This is because the decrease in surface area of the specimen with increasing E_a is suppressed on SiO_2-coated specimen due to the formation of thinner anodic oxide films with higher electric field sustainability. The capacitance of E_a=1,000 V anodic oxide films formed on SiO_2-coated specimen is 39% higher than that on non-coated specimen.

Conclusively, electrophoretic coating of SiO_2 on DC-etched aluminum before anodizing is very effective to increase the capacitance of anodic oxide films at high voltage.

Conclusion

Electrophoretic sol-gel coating of SiO_2 was performed on DC-etched and electropolished aluminum, and then anodizing was carried out to examine the dielectric properties of anodic oxide films. The following conclusions may be drawn.

1. Electrophoretic sol-gel coating can form SiO_2 films uniformly on the surface of plain and DC-etched specimens. A thin oxide layer is formed by anodic oxidation during the formation of SiO_2 film.
2. Anodizing of aluminum coated with SiO_2 films leads to the formation of oxide films, which consist of an outer

Al–Si composite oxide layer and an inner Al2O3 layer underneath SiO2 layer. The anodic oxide films formed, thus, has a high electric field sustainability.

3. The anodic oxide films formed on specimens with SiO2 film in a boric acid/borate solution have at most 10% higher parallel capacitance than those without SiO2 layer. Higher heating temperatures after electrophoretic deposition lead to the increase in capacitance of anodic oxide films.
4. The parallel capacitance of anodic oxide films formed in a boric acid solution on DC-etched specimens with SiO2 film is 39% higher at Ea=1,000 V than that on electropolished specimens due to the suppression of the decrease in the surface area by forming thinner anodic oxide films with a higher electric field sustainability.

References

1. Takahashi H, Umehara Y, Miyamoto T, Fujimoto N, Nagayama M (1987) J Metal Fin Soc Jpn 38:67–73
2. Takahashi H, Umehara Y, Nagayama M (1987) J Metal Fin Soc Jpn 38:139–142
3. Takahashi H, Umehara Y, Furuichi R, Nagayama M (1989) J Metal Fin Soc Jpn 40:590–597
4. Takahashi H, Takahashi K, Furuichi R, Nagayama M (1989) J Metal Fin Soc Jpn 40:1415–1421
5. Takahashi H, Ikegami C, Seo M, Furuichi R (1991) J Electron Microsc 40:101–109
6. Takahashi H, Dairaku M, Seo M (1994) J Surf Fin Soc Jpn 45:810–817
7. Shikanai M, Sakairi M, Takahashi H, Seo M, Takahiro K, Nagata S, Yamaguchi S (1997) J Electrochem Soc 144:2756–2766
8. Takahashi H, Kamada H, Sakairi M, Takahiro K, Nagata S, Yamaguchi S (1998) Proc Intern Symp of Dielectric Material Integration for Micro Electronics, sponsored by Electrochem Soc, pp 253–262
9. Tian H-Y, Luo W-G (2001) Mater Chem Phys 69:166–171
10. Nayak M, Lee SY, Tseng T-Y (2002) Mater Chem Phys 77:34–42
11. Adikary SU, Chan HLW (2003) Thin Solid Films 424:70–74
12. Xu Y (2004) Ceram Int 30:1741–1743
13. Park S-S, Lee B-T (2004) J Electroceramics 13:111–116
14. Watanabe K, Sakairi M, Takahashi H, Hirai S, Yamaguchi S (1999) J Surf Fin Soc Jpn 50:359–366
15. Watanabe K, Sakairi M, Takahashi H, Hirai S, Yamaguchi S (1999) J Electroanal Chem 473:250–255
16. Watanabe K, Sakairi M, Takahashi H, Takahiro K, Nagata S, Hirai S (1999) Electrochemistry 67:1243–1248
17. Watanabe K, Sakairi M, Takahashi H, Takahiro K, Nagata S, Hirai S (2001) Electrochemistry 69:407–413
18. Watanabe K, Sakairi M, Takahashi H, Takahiro K, Nagata S, Hirai S (2001) J Electrochem Soc 148:B473–B481
19. Watanabe K, Sakairi M, Takahashi H, Hirai S (2003) Materia 42:911
20. Takahashi H, Sakairi M, Watanabe K, Kikuchi T, Yamada M (2003) J Surf Fin Soc Jpn 54(7):436–441
21. Watanabe K, Sakairi M, Takahashi H, Hirai S (2003) J Surf Fin Soc Jpn 54(3):235–240
22. Watanabe K, Sakairi M, Takahashi H, Nagata S, Hirai S (2004) J Surf Fin Soc Jpn 55:471–477
23. Hasegawa K, Tatsumisago M, Inami T (1997) J Ceramic Soc Jpn 105:569
24. Sakka S (1996) Science of sol-gel method, p 8 (Agne-shouhusha)
25. Zhang RF, Ma J, Kong LB (2002) J Mater Res 17:933–935
26. Li Y, Shimada H, Sakairi M, Shigyo K, Takahashi H, Seo M (1997) J Electrochem Soc 144:866–876
27. Shimada H, Sakairi M, Takahashi H (2002) J Surf Fin Soc Jpn 53:134–141
28. Shimada H, Sakairi M, Takahashi H (2002) J Surf Fin Soc 53:142–148